Title
Regulation of Substrate Utilization by the Mitochondrial Pyruvate Carrier

Journal
Molecular Cell, 56(5)

ISSN
1097-2765

Authors
Vacanti, Nathaniel M
Divakaruni, Ajit S
Green, Courtney R
et al.

Publication Date
2014-12-01

DOI
10.1016/j.molcel.2014.11.017

Peer reviewed

Molecular Cell
Article

CellPress

Regulation of Substrate Utilization by the Mitochondrial Pyruvate Carrier

Nathaniel M. Vacanti,[1] Ajit S. Divakaruni,[2] Courtney R. Green,[1] Seth J. Parker,[1] Robert R. Henry,[3,4] Theodore P. Ciaraldi,[3,4] Anne N. Murphy,[2] and Christian M. Metallo[1,*]
[1]Department of Bioengineering, University of California, San Diego, La Jolla, CA 92093, USA
[2]Department of Pharmacology, University of California, San Diego, La Jolla, CA 92093, USA
[3]Department of Medicine, University of California, San Diego, La Jolla, CA 92093, USA
[4]VA San Diego Healthcare System, San Diego, CA 92162, USA
*Correspondence: cmetallo@ucsd.edu
http://dx.doi.org/10.1016/j.molcel.2014.09.024

SUMMARY

Pyruvate lies at a central biochemical node connecting carbohydrate, amino acid, and fatty acid metabolism, and the regulation of pyruvate flux into mitochondria represents a critical step in intermediary metabolism impacting numerous diseases. To characterize changes in mitochondrial substrate utilization in the context of compromised mitochondrial pyruvate transport, we applied ^{13}C metabolic flux analysis (MFA) to cells after transcriptional or pharmacological inhibition of the mitochondrial pyruvate carrier (MPC). Despite profound suppression of both glucose and pyruvate oxidation, cell growth, oxygen consumption, and tricarboxylic acid (TCA) metabolism were surprisingly maintained. Oxidative TCA flux was achieved through enhanced reliance on glutaminolysis through malic enzyme and pyruvate dehydrogenase (PDH) as well as fatty acid and branched-chain amino acid oxidation. Thus, in contrast to inhibition of complex I or PDH, suppression of pyruvate transport induces a form of metabolic flexibility associated with the use of lipids and amino acids as catabolic and anabolic fuels.

INTRODUCTION

Mitochondria execute core metabolic functions in eukaryotes ranging from catabolic energy conversion to anabolism of biosynthetic intermediates. Cells must negotiate their nutritional environment to control which substrates are metabolized in mitochondria while continuing to meet their bioenergetic and/or biosynthetic needs. Pyruvate lies at the intersection of glycolysis, gluconeogenesis, and the tricarboxylic acid (TCA) cycle; as such, its transport into the mitochondrial matrix influences carbohydrate, fatty acid, and amino acid metabolism. Dysregulation of these processes contributes to the pathogenesis of numerous diseases, including diabetes and obesity (DeFronzo and Tripathy, 2009; Sugden et al., 2009), mitochondrial disorders (Kerr, 2013), cardiac failure (Fillmore and Lopaschuk, 2013), neurodegenerative disorders (Cunnane et al., 2011; Yao et al., 2011), and cancer (Currie et al., 2013; Tennant et al., 2010). Therefore, strategies that modulate the extent of pyruvate flux into mitochondrial pathways may have therapeutic potential by directly or indirectly affecting glucose, lipid, and/or amino acid homeostasis in the body.

Existence of a protein carrier to facilitate pyruvate transport into mitochondria has been recognized for decades (Halestrap and Denton, 1974; Papa et al., 1971). Although activity of this transporter and sensitivity to inhibitors have been characterized (Clark and Land, 1974; Halestrap and Denton, 1974; Papa and Paradies, 1974), the genes encoding this complex remained a mystery for many years. Two recent studies revealed strong evidence that the genes, renamed *MPC1* and *MPC2*, encode the multimeric mitochondrial pyruvate carrier (MPC) complex embedded in the mitochondrial inner mitochondrial membrane (Bricker et al., 2012; Herzig et al., 2012). Indeed, Herzig et al. (2012) observed that coexpression of *Mpc1* and *Mpc2* in *Lactococcus lactis* induced a 4-fold increase in pyruvate uptake. Consistent with these results, Bricker et al. (2012) described the functional redundancy of MPC across several species (yeast, *Drosophila*, human) and identified a mutation in *MPC1* that confers resistance to inhibition by the α-cyanocinnamate analog UK5099 (Halestrap, 1975). These discoveries provide an exciting potential drug target through which mitochondrial substrate utilization may be controlled in the context of metabolic disorders. In fact, the MPC has emerged as an unanticipated target of thiazolidinediones (Colca et al., 2013; Divakaruni et al., 2013), a class of insulin sensitizing drugs, and as a regulator of insulin secretion (Patterson et al., 2014; Vigueira et al., 2014), suggesting that this transporter plays a central role in substrate selection and metabolic signaling. Moreover, recent work shows that the phosphodiesterase inhibitor Zaprinast can alter aspartate and glutamate metabolism via the MPC (Du et al., 2013) and glutaminase (Elhammali et al., 2014).

The high biosynthetic and energetic demands of skeletal muscle myoblasts render them an ideal system to characterize the influence of mitochondrial pyruvate carrier function on metabolic flux and substrate selection. This study examines metabolic flux regulation by MPC in the context of the metabolic network in intact cells. *Mpc1* or *Mpc2* was chronically suppressed using lentiviral-mediated delivery of shRNAs and/or pharmacologically inhibited with UK5099 in both proliferating and differentiated mouse C2C12 muscle cells, several human transformed cell

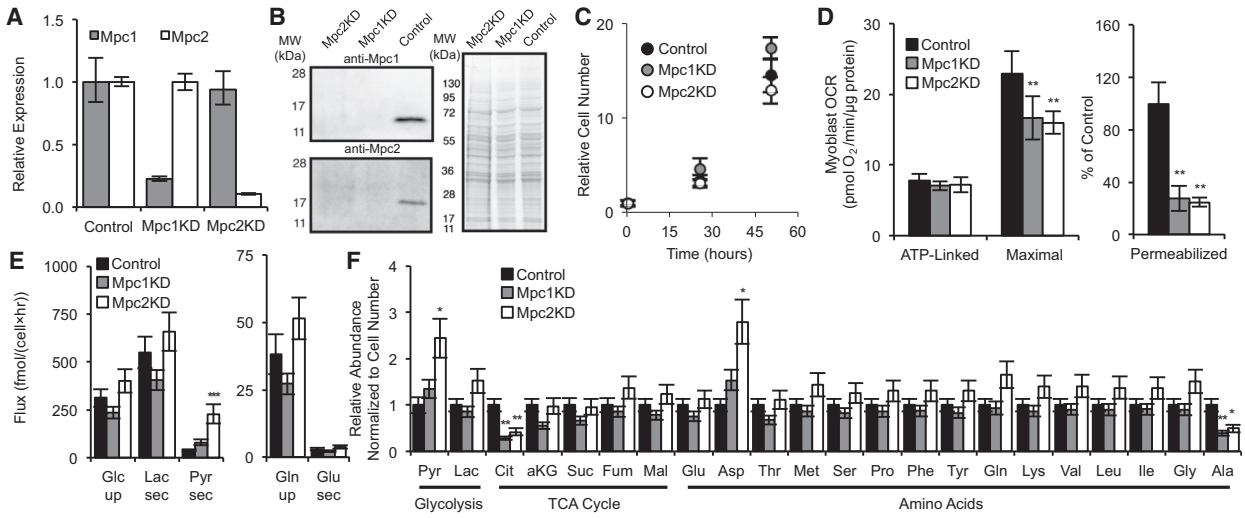

Figure 1. MPC Knockdown Does Not Affect the Overall Metabolic State of Cells

(A and B) Relative expression of *Mpc1* and *Mpc2* as determined by qPCR (A) and western blot (B).

(C–E) Proliferation (C), oxygen consumption rates (OCRs; D), and extracellular substrate fluxes (E) of control, Mpc1KD, and Mpc2KD cells. (D) ATP-linked and maximal respiration of intact cells and pyruvate-dependent respiration in permeabilized cells (measured as outlined in Experimental Procedures).

(F) Relative abundance of intracellular metabolites.

Error bars represent minimum and maximum relative expression as calculated by qPCR data analysis software (A), standard deviation (SD) (C, E, and F), or standard error of the mean (SEM) (D). *p < 0.05, **p < 0.01, and ***p < 0.001 by ANOVA with Dunnett's post hoc test.

lines, and primary human skeletal myotubes (hSKMs). Surprisingly, proliferating myoblasts maintained growth and ATP-linked respiration despite profound inhibition of MPC activity; however, reliance on substrates for energy and biosynthetic metabolism shifted from glucose to amino acid and fatty acid oxidation. TCA flux and fatty acid synthesis were maintained through increased glutamine anaplerosis and oxidation, malic enzyme flux, and fatty acid oxidation. Finally, pharmacological inhibition of MPC activity in hSKMs increased the extent that branched-chain amino acids (BCAAs) were oxidized in the TCA cycle.

RESULTS

Proliferation and Oxidative Metabolism Are Maintained upon *Mpc* Depletion

To investigate how metabolism is reprogrammed in response to MPC inhibition, we depleted Mpc levels in C2C12 myoblasts using targeting *Mpc1* (Mpc1KD), *Mpc2* (Mpc2KD), or control sequences (control). Stable knockdown was confirmed at the transcriptional and protein levels (Figures 1A and 1B). Despite the importance of glucose and pyruvate metabolism for biosynthesis and ATP generation, cell proliferation rates and ATP-linked respiration were unaffected by the absence of Mpc1 and Mpc2 (Figures 1C and 1D). In fact, *Mpc* knockdown only influenced oxygen consumption in the uncoupled state when all substrates were present, while pyruvate-dependent respiration in permeabilized cells was significantly compromised (Figure 1D). Surprisingly, *Mpc* knockdown had little effect on glucose and glutamine uptake, as well as lactate and glutamate secretion, though pyruvate secretion was significantly increased (Figure 1E).

We next performed a targeted metabolomic analysis to gain more insight into the intracellular metabolic changes occurring upon Mpc depletion (Figure 1F). Intracellular pyruvate was elevated upon *Mpc* knockdown, whereas the abundances of most TCA cycle intermediates were unaffected. Citrate levels, however, were markedly decreased in Mpc1KD or Mpc2KD (Mpc1/2KD) cells, as this metabolite is generated predominantly from pyruvate-derived AcCoA under normal growth conditions (Metallo et al., 2012). Aspartate and alanine abundances were significantly increased and decreased, respectively, suggesting that amino acid metabolism was altered to maintain metabolic homeostasis.

Oxidative Glutaminolysis Supports the TCA Cycle in Cells Lacking Mpc

To gain more detailed insights into mitochondrial substrate utilization, we cultured cells in the presence of [U-$^{13}C_6$]glucose for 24 hr and observed steady-state isotopic labeling (Figure S1A, available online). Consistent with the expected decrease in glucose-derived pyruvate oxidation, labeling of citrate and all TCA intermediates was significantly decreased in Mpc1/2KD cells relative to controls (Figures 2A and 2B). While the relative abundances of fully labeled (M3) lactate and pyruvate were unchanged in Mpc1/2KD cells, the extent of alanine labeling from [U-$^{13}C_6$]glucose was significantly decreased (Figure 2C). Additionally, we observed an increase in de novo serine synthesis from glucose in the cytosol (Figure 2D), highlighting potential compartment-specific shifts in amino acid metabolism (Figure S1B).

Next, we cultured C2C12 myoblasts in the presence of [U-$^{13}C_5$]glutamine to detect changes in glutamine utilization in the context of decreased Mpc function. The abundance of fully labeled succinate, fumarate, α-ketoglutarate, and malate increased significantly in Mpc1/2KD cells (Figure 2E), suggesting that cells increase their reliance on glutamine anaplerosis when

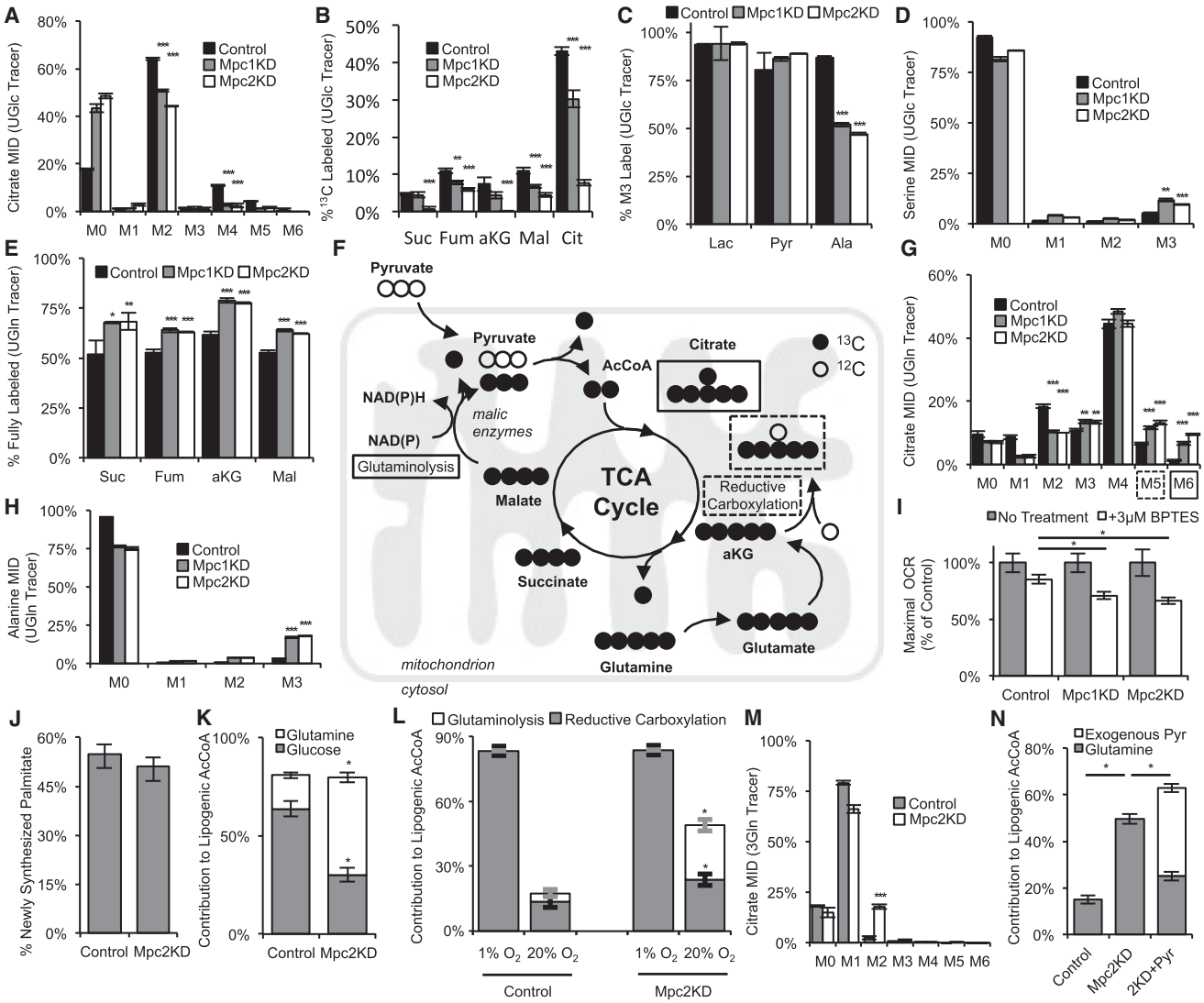

Figure 2. MPC Regulates Mitochondrial Substrate Utilization

(A) Citrate mass isotopomer distribution (MID) resulting from culture with [U-$^{13}C_6$]glucose (UGlc).

(B) Percentage of ^{13}C-labeled metabolites from UGlc.

(C) Percentage of fully labeled lactate, pyruvate, and alanine from UGlc.

(D) Serine MID resulting from culture with UGlc.

(E) Percentage of fully labeled metabolites derived from [U-$^{13}C_5$]glutamine (UGln).

(F) Schematic of UGln labeling of carbon atoms in TCA cycle intermediates arising via glutaminolysis and reductive carboxylation. Mitochondrion schematic inspired by Lewis et al. (2014).

(G and H) Citrate (G) and alanine (H) MIDs resulting from culture with UGln.

(I) Maximal oxygen consumption rates with or without 3 μM BPTES in medium supplemented with 1 mM pyruvate.

(J) Percentage of newly synthesized palmitate as determined by ISA.

(K) Contribution of UGln and UGlc to lipogenic AcCoA as determined by ISA.

(L) Contribution of glutamine to lipogenic AcCoA via glutaminolysis (ISA using a [3-^{13}C]glutamine [3Gln]) and reductive carboxylation (ISA using a [5-^{13}C]glutamine [5Gln]) under normoxia and hypoxia.

(M) Citrate MID resulting from culture with 3Gln.

(N) Contribution of UGln and exogenous [3-^{13}C]pyruvate (3Pyr) to lipogenic AcCoA. 2KD+Pyr refers to Mpc2KD cells cultured with 10 mM extracellular pyruvate. Error bars represent SD (A–E, G, H, and M), SEM (I), or 95% confidence intervals (J–L, and N). *$p < 0.05$, **$p < 0.01$, and ***$p < 0.001$ by ANOVA with Dunnett's post hoc test (A–E and G–I) or * indicates significance by nonoverlapping 95% confidence intervals (J–L and N).

mitochondrial pyruvate transport is limited. Isotopic enrichment in citrate provides additional insight into the reprogramming of TCA metabolism. Increased M5 citrate abundance from [U-$^{13}C_5$]glutamine can arise via reductive carboxylation by isocitrate dehydrogenase (IDH) enzymes, and M6 citrate arises through the combined activity of glutaminolysis and pyruvate dehydrogenase

(Figure 2F) (Le et al., 2012; Metallo and Vander Heiden, 2013). In the glutaminolysis pathway, glutamine is oxidized in the mitochondria and converted to pyruvate via malic enzymes (MEs). AcCoA is then generated by the PDH complex and condenses with oxaloacetate to form citrate (Figure 2F). The relative abundances of both M5 and M6 mass isotopomers were significantly increased in Mpc1/2KD cells (Figure 2G). Furthermore, the abundance of glutamine-derived alanine was significantly elevated (Figure 2H), consistent with higher flux through mitochondrial MEs as opposed to reductive carboxylation.

To further highlight the increased role of glutaminolysis in cells with *Mpc* knockdown, we measured uncoupled respiration in the absence or presence of the glutaminase inhibitor, bis-2-(5-phenylacetamido-1,3,4-thiazol-2-yl)ethyl sulfide (BPTES). Uncoupler-stimulated respiration in Mpc1/2KD cells was more sensitive to BPTES treatment, signifying an increased reliance on glutamine oxidation in these cells (Figure 2I). Collectively, these results provide evidence that cells with depleted Mpc1 or Mpc2 increase oxidative glutamine metabolism to maintain flux through the TCA cycle.

Mpc Knockdown Induces Substrate Switching for De Novo Lipogenesis

We next quantified isotope enrichment in palmitate and performed isotopomer spectral analysis (ISA) to determine (1) the percent of newly synthesized palmitate after tracer addition and (2) the relative contribution of glucose and glutamine to lipogenic AcCoA (Kharroubi et al., 1992; Metallo et al., 2012). Although we observed no significant change in relative palmitate synthesis upon Mpc depletion (Figure 2J), the extent of glutamine conversion to the lipogenic AcCoA pool was significantly increased in Mpc2KD cells (Figure 2K). Glutamine can contribute carbon to fatty acid synthesis via reductive carboxylation or oxidative glutaminolysis. The former pathway is highly active in cells proliferating under hypoxia or those with a compromised respiratory chain (Metallo et al., 2012; Mullen et al., 2012; Scott et al., 2011; Wise et al., 2011), while the latter pathway has been observed in B cell lymphoma (Le et al., 2012). While the contribution of glutamine flux through reductive carboxylation to lipogenesis increased in control and Mpc2KD cells cultured under hypoxia (measured specifically using [5-^{13}C]glutamine (Yoo et al., 2008), flux through this pathway did not account for the increased glutamine-derived AcCoA in Mpc2KD cells grown under normoxia. The increased glutamine-derived AcCoA was almost exclusively attributed to the glutaminolysis pathway, as evidenced by transfer of label from [3-^{13}C]glutamine to palmitate (Figures 2L and S1C). We also measured a significant increase in M2 labeling of citrate in Mpc2KD myoblasts cultured with [3-^{13}C]glutamine (Figure 2M), which arises from condensation of labeled oxaloacetate and AcCoA (Figure S1C). No change in labeling was observed in lactate (Figure S1D), providing evidence that this ME flux was catalyzed within the mitochondrial compartment. These results demonstrate that *Mpc* knockdown causes metabolic reprogramming that is distinct from hypoxia-associated PDH inhibition (Kim et al., 2006; Papandreou et al., 2006), with an increased proportion of mitochondrial AcCoA derived from mitochondrial ME and PDH activity rather than reductive carboxylation.

At high concentrations, pyruvate passively enters the matrix, bypassing the MPC (Bakker and van Dam, 1974; Halestrap, 1975). To further demonstrate that PDH activity is maintained in *Mpc* knockdown cells, we quantified how glutamine to AcCoA conversion was affected by exogenous pyruvate. In the presence of 10 mM extracellular pyruvate, Mpc2KD cells failed to increase the contribution of glutamine carbon to palmitate synthesis. Indeed, this difference was entirely accounted for by the conversion of exogenous [3-^{13}C]pyruvate to lipogenic AcCoA through the PDH complex (Figure 2N).

Amino Acid and β-Oxidation Fuel Mitochondrial Metabolism upon *Mpc* Knockdown

To quantify changes in intracellular fluxes in a more unbiased and comprehensive manner, we conducted ^{13}C MFA on Mpc2KD and control cells. Steady-state mass isotopomer distributions (MIDs) measured in cells cultured with [U-$^{13}C_5$]glutamine and [1,2-$^{13}C_2$]glucose along with independently determined uptake/secretion fluxes were incorporated into a model of central carbon metabolism (Ahn and Antoniewicz, 2011; Murphy et al., 2013). The INCA software suite was used to estimate fluxes and associated confidence intervals using an elementary metabolite unit-based algorithm (Antoniewicz et al., 2006; Young, 2014). Results are illustrated in Figures 3A, S2A, and S2B and tabulated in Tables S1 and S2; a detailed description of the model, data, and assumptions are included in the Supplemental Experimental Procedures and in Table S3. Flux data indicated that mitochondrial pyruvate transport and PDH flux decreased significantly upon *Mpc2* knockdown. Oxidative TCA flux through IDH was also decreased with no absolute increase in reductive carboxylation flux, while pyruvate cycling and glutaminolytic flux were increased. Increased flux through mitochondrial MEs at least partially sustained AcCoA metabolism. Intriguingly, an acceptable fit for *Mpc2* knockdown cells could only be obtained when an exogenous source of AcCoA was included in the model. Flux from this AcCoA pool into the TCA cycle increased 5-fold in Mpc2KD cells compared to control cells, suggesting that oxidation of mitochondrial substrates other than glutamine were also induced upon Mpc depletion (Figure 3A and Tables S1 and S2).

Given the lack of branched-chain amino acid (BCAA) oxidation to TCA intermediates observed in both control and Mpc2KD cells (Figure S2C), we hypothesized that this AcCoA was derived from β-oxidation. To more explicitly determine if *Mpc* knockdown drives an increase in fatty acid oxidation, we cultured Mpc2KD and control cells in the presence of [U-$^{13}C_{16}$]palmitate bound to BSA and observed ^{13}C enrichment in TCA intermediates. We observed a significant increase in the relative abundance of M2 citrate from this tracer in Mpc2KD compared to control cells (Figure 3B). Increased label incorporation into numerous TCA metabolites downstream of citrate was also detected (Figure 3C), indicating that knockdown of *Mpc2* induced a significant increase in fatty acid oxidation flux in C2C12 myoblasts.

To confirm the observed metabolic shifts in mitochondrial substrate utilization in an orthogonal manner, we quantified the ATP-linked and maximal respiration of each cell line in the presence of either or both BPTES and etomoxir. The former compound inhibits glutamine oxidation via glutaminase, whereas the latter inhibits fatty acid oxidation at carnitine palmitoyltransferase-1

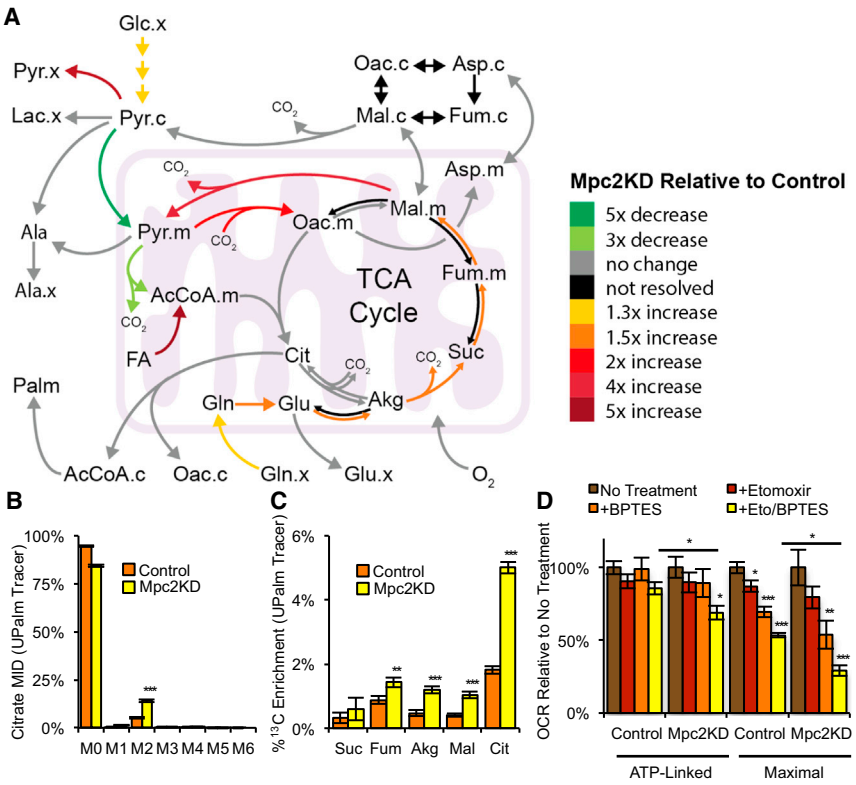

Figure 3. Mpc Knockdown Increases Fatty Acid Oxidation

(A) Schematic of changes in flux through metabolic pathways in Mpc2KD relative to control cells.

(B) Citrate MID resulting from culture with [U-$^{13}C_{16}$] palmitate conjugated to BSA (UPalm).

(C) Percentage of ^{13}C enrichment resulting from culture with UPalm.

(D) ATP-linked and maximal oxygen consumption rate, with or without 20 μM etomoxir, with or without 3 μM BPTES. Culture medium supplemented with 0.5 mM carnitine.

Error bars represent SD (B and C) or SEM (D). *$p < 0.05$, **$p < 0.01$, and ***$p < 0.001$ by two-tailed, equal variance, Student's t test (B–D), or by ANOVA with Dunnett's post hoc test (D).

(CPT1). ATP-linked respiration was only affected when all three pathways (i.e., pyruvate transport, glutamine, and fatty acid oxidation) were inhibited (Figures 1D, 3D, and S2D for raw values). On the other hand, maximal respiration was significantly decreased by each individual treatment, with the most pronounced effect being observed when BPTES and etomoxir were both added to the culture (Figures 1D, 3D, and S2E for raw values). The synergistic effect of inhibiting these three mitochondrial substrate oxidation pathways highlights the plasticity of mitochondrial metabolism in respiring cells and independently demonstrates that Mpc depletion potentiates cells to employ fatty acid and amino acid oxidation to meet their bioenergetic demands.

Small Molecule Inhibition of MPC Enhances Amino Acid and Fatty Acid Oxidation

Pharmacological inhibition of Mpc function rather than shRNAs may provide a more clinically relevant means of exploiting mitochondrial flexibility. To determine whether small molecules targeting the Mpc elicit effects similar to that of inhibition at the transcriptional level, we treated cells with UK5099, which covalently binds to Mpc and blocks pyruvate transport (Hildyard et al., 2005). Culture of proliferating C2C12 cells for 24 hr with 10 μM UK5099 in the presence of [U-$^{13}C_6$]glucose revealed a relative decrease in glucose flux to the TCA cycle, and results using [U-$^{13}C_5$]glutamine indicate that glutaminolytic flux through malic enzyme was significantly increased, as evidenced by the relative abundance of M6 citrate (Figures 4A and 4B). As observed in the comparison to hypoxia (Figure 2L), the metabolic response to UK5099 treatment is distinct from that occurring in response to complex I inhibition. Whereas oxidative TCA flux is maintained during UK5099 treatment, rotenone, a potent inhibitor of complex I, shuts down oxidative glutamine metabolism and increases reductive carboxylation activity, resulting in a dramatic increase in the relative abundance of M5 citrate from [U-$^{13}C_5$]glutamine (Figure 4B). C2C12 myoblasts also displayed a shift away from glucose to glutamine as a substrate for fatty acid synthesis in the presence of UK5099 (Figure 4C).

Additionally, ATP-linked and uncoupled oxygen consumption were measured when C2C12 cells were cultured for 24 hr with UK5099 to examine their dependency on different oxidative substrates. We observed no change in ATP-linked or maximal respiration with UK5099 treatment, presumably due to the metabolic plasticity of cells when other pathways (i.e., glutamine and fatty acid oxidation) were not inhibited (Figures 4D, S2F, and S2G for raw values). However, when cells were treated with combinations of UK5099, BPTES, and etomoxir, we detected a significant effect of UK5099 only with combinatorial treatments (Figures 4D, S2F, and S2G for raw values). These results further highlight the flexibility of oxidative mitochondrial metabolism that can be induced by Mpc inhibition such that C2C12 cells meet their energetic demands through glutamine and fatty acid oxidation.

Proliferating Human Transformed Cells Reprogram Metabolism upon MPC Inhibition

To validate these findings in human cells using independent shRNAs, MPC levels were also depleted in A549 carcinoma cells using shRNAs targeting *MPC1* (MPC1KD), *MPC2* (MPC2KD), or a control sequence. These cells were cultured with [U-$^{13}C_6$]glucose, [U-$^{13}C_5$]glutamine, and [U-$^{13}C_{16}$]palmitate-BSA to observe metabolic reprogramming in response to MPC depletion. Results supported findings in C2C12 myoblasts, as glucose conversion to citrate, TCA intermediates, and alanine were all significantly decreased in MPC1/2KD A549 cells (Figures S3A–S3C). On the

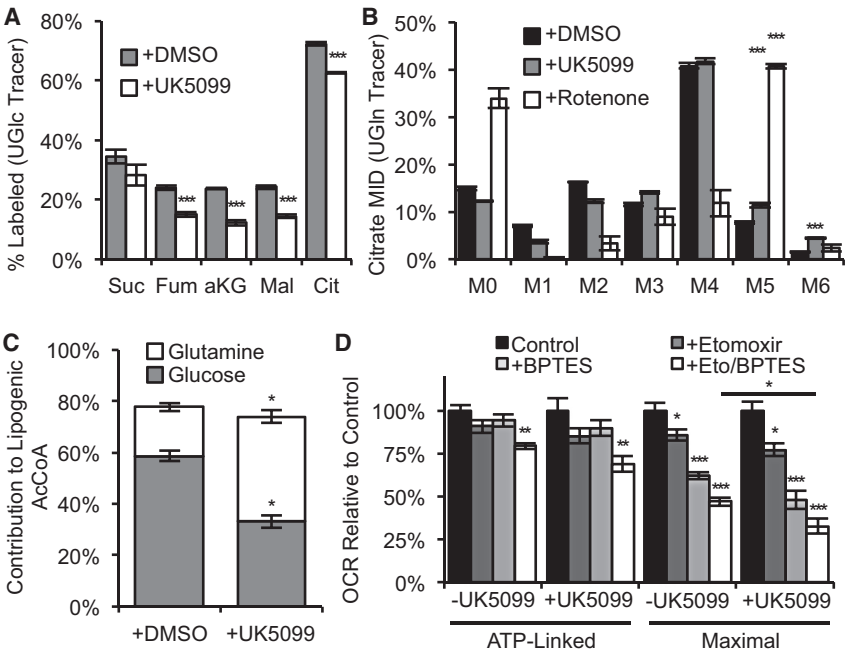

Figure 4. Metabolic Reprogramming Resulting from Pharmacological Mpc Inhibition Is Distinct from Hypoxia or Complex I Inhibition

(A) Percentage of ^{13}C-labeled metabolites from UGlc, with or without 10 μM UK5099.

(B) Citrate MID resulting from culture with UGln, with or without 10 μM UK5099 or with or without 30 nM rotenone.

(C) Relative contribution of UGlc and UGln to lipogenic AcCoA, with or without 10 μM UK5099.

(D) ATP-linked and maximal oxygen consumption rate, with or without 10 μM UK5099, with or without 20 μM etomoxir, and with or without 3 μM BPTES. Culture medium supplemented with 0.5 mM carnitine.

Cells were pretreated with 10 μm UK5099 (A and C). Error bars represent SD (A and B), 95% confidence intervals (C), or SEM (D). *$p < 0.05$, **$p < 0.01$, and ***$p < 0.001$ by two-tailed, equal variance, Student's t test (A and D), by ANOVA with Dunnett's post hoc test (B and D) or * indicates significance by nonoverlapping 95% confidence intervals (C).

other hand, glutamine anaplerosis and oxidation through malic enzymes were elevated upon *MPC* knockdown in these cells, as evidenced by labeling of TCA intermediates (citrate in particular) and alanine from [U-$^{13}C_5$]glutamine and [3-^{13}C]glutamine (Figures S3D–S3G). Finally, we observed that MPC1KD A549 cells exhibited an increased reliance on fatty acid oxidation to fuel TCA cycle metabolism, as ^{13}C labeling of citrate and other TCA metabolites derived from [U-^{13}C]palmitate increased significantly (Figures S3H and S3I). A549 cells also responded to pharmacological inhibition of MPC by UK5099, as glucose contribution to the TCA cycle declined (Figure S3J) and glutamine oxidation increased (Figure S3K). Finally, both A549 cells and the Huh7 human hepatocarcinoma cell line increased their reliance on fatty acid oxidation to fuel TCA metabolism upon MPC inhibition (Figures S3L and S3M).

MPC Influences Mitochondrial Substrate Utilization in Differentiated Myotubes

To determine whether Mpc functions similarly in more differentiated cells, we formed myotubes using control, Mpc1KD, and Mpc2KD C2C12 cells via 4-day treatments with 2% horse serum. Differentiation was confirmed by observing elongation and fusion of myoblasts to form multinucleated tubes using light microscopy and by immunofluorescent staining of desmin, a marker of differentiated muscle (Figure S4A). Maintenance of the knockdown upon differentiation was confirmed at the protein and mRNA levels (Figures 5A and 5B). Knockdown of *Mpc* did not affect glycolytic flux in C2C12 myotubes, as lactate secretion, glucose uptake, and the ratio of the two were surprisingly unchanged (Figure 5C). Furthermore, respiratory inhibition of intact cells presented with all substrates was evident only when oxidative phosphorylation was uncoupled, yet Mpc activity was clearly compromised as indicated by a decreased rate of pyruvate-driven respiration in permeabilized myotubes (Figure 5D).

Targeted metabolomic analysis revealed increases in intracellular abundances of pyruvate and aspartate in Mpc2KD myotubes (Figure S4B). In contrast to proliferating cells, myotubes rely primarily on glucose carbon for the generation of TCA intermediates (rather than glutamine) (Figure S4C). To better resolve changes in pyruvate metabolism upon *Mpc* knockdown or inhibition, we cultured myotubes in the presence of either [U-$^{13}C_6$]glucose or [3-^{13}C]pyruvate for 2 hr before quantifying isotopic labeling in TCA intermediates. Enrichment of glucose and pyruvate carbons in the TCA cycle was significantly decreased in response to UK5099 treatment (Figures 5E and 5F) or when comparing Mpc2KD to control myotubes (Figures S4D and S4E). Importantly, the pool sizes of all intermediates shown was less than or equal to those quantified in controls. As such, the decreased labeling observed under non-steady-state conditions is indicative of decreases in metabolic flux (rather than pool size changes). Additionally, we observed a significant increase in glutaminolysis in C2C12 myotubes treated with UK5099, as evidenced by steady-state labeling from [U-$^{13}C_5$]glutamine (Figure 5G). Similar trends were observed in myotubes generated using control or Mpc2KD cells (Figure S4F). Although the lower metabolic rate of nonproliferating myotubes (compared to proliferating cells) minimized the observed differences and limited our ability to quantify fatty acid oxidation in these cultures, results indicate that Mpc inhibition induces differentiated myotubes to increase glutamine oxidation.

Whereas glutamine is an important substrate for proliferating cells, BCAAs are critical bioenergetic substrates for muscle and other tissues, particularly in the fasted state (Rosenthal et al., 1974). BCAAs have recently been demonstrated to accumulate in the context of obesity and insulin resistance (Adams, 2011; Newgard et al., 2009; Wang et al., 2011), though the mechanisms leading to this metabolic phenotype (i.e., higher intake, decreased catabolism) are not yet clear. We failed to detect

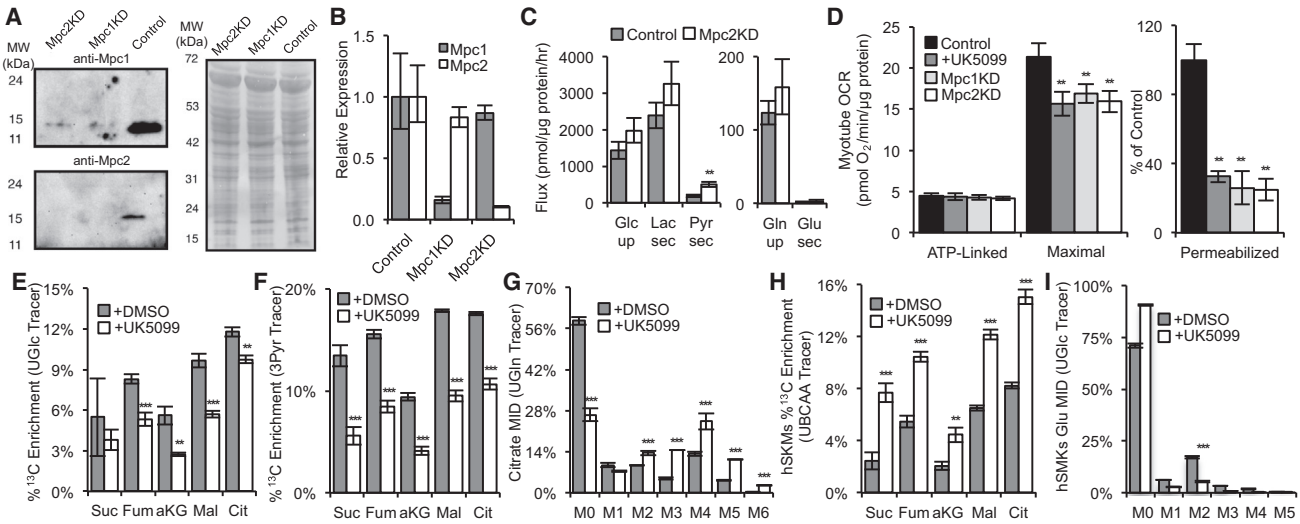

Figure 5. Mpc Controls Oxidative Substrate Utilization in Myotubes

(A and B) Protein (A) and mRNA (B) levels of Mpc1 and Mpc2.

(C) Extracellular substrate fluxes in Control or Mpc2KD C2C12 myotubes.

(D) ATP-linked and maximal OCR of intact C2C12 myotubes and pyruvate-dependent OCR of permeabilized C2C12 myotubes.

(E and F) Percentage of ^{13}C enrichment resulting from culture of C2C12 myotubes with UGlc (E) and 3Pyr (F) for 2 hr, with or without 5 μM UK5099.

(G) Citrate MID resulting from culture of C2C12 myotubes with UGln, with or without 10 μM UK5099.

(H) Percentage of ^{13}C enrichment in patient 1 hSKMs cultured with [U-$^{13}C_5$]valine, [U-$^{13}C_6$]leucine, and [U-$^{13}C_6$]isoleucine (collectively UBCAA), with or without 10 μM UK5099.

(I) hSKMs glutamate MID resulting from culture with [U-$^{13}C_6$]glucose, with or without 10 μM UK5099.

Error bars represent minimum and maximum relative expression as calculated by qPCR data analysis software (B), SD (C and E–I), or SEM (D). *$p < 0.05$, **$p < 0.01$, and ***$p < 0.001$ by a two-tailed, equal variance, Student's t test (C and E–I), or by ANOVA with Dunnett's post hoc test (D).

significant flux through this pathway in any of the C2C12 myoblasts (Figure S2C), myotubes, or engineered lines generated here using [^{13}C]BCAA tracers. To determine whether MPC inhibition promoted BCAA catabolism in a more physiologically relevant system, we cultured hSKMs in medium containing [U-$^{13}C_5$]valine, [U-$^{13}C_6$]leucine, and [U-$^{13}C_6$]isoleucine in the presence or absence of UK5099. Notably, ^{13}C enrichment throughout the TCA cycle was significantly increased in hSKMs treated with 10 μM UK5099 compared to controls (Figures 5H and S4G). As expected, glucose oxidation was inhibited in hSKMs cultured with UK5099 (Figure 5I). Consistent increases in BCAA oxidation were observed in hSKMs obtained from two independent subjects (Figures 5H and S4G). These results suggest that mitochondrial substrate utilization can be controlled in terminally differentiated hSKMs by modulating Mpc activity to influence BCAA catabolism.

DISCUSSION

Traditional approaches to modulate eukaryotic cell metabolism have focused on controlling enzyme activity and/or expression. Such treatments can cause bottlenecks and place constraints on cells that limit metabolism globally. Since metabolic processes in eukaryotes are segregated within the mitochondrial matrix, cytosol, and other subcellular compartments, an alternate approach may be to target compartment-specific transporters and exploit the inherent metabolic flexibility of cells to control substrate utilization. In this manner, cells and tissues that pathologically rely on particular nutrients (e.g., anabolic glucose metabolism in diabetes, obesity, and cancer) may be coaxed to shift toward a catabolic state of metabolism while maintaining enzyme activity throughout the cell. A critical step in this process is to functionally characterize how substrate utilization and intracellular metabolic activity (i.e., fluxes) are reprogrammed upon inhibition of specific transporters (Zamboni et al., 2009). Here we have outlined the metabolic phenotype of cell lines and hSKMs that emerge upon inhibition of the mitochondrial pyruvate transporter encoded by *MPC1* and *MPC2*. The observed changes in substrate utilization provide some insights through which MPC inhibition can elicit beneficial effects via reprogramming of mitochondrial metabolism.

Knockdown of either *Mpc1* or *Mpc2* abrogated expression of both proteins, as observed previously (Divakaruni et al., 2013). Comprehensive ^{13}C MFA integrating data from parallel tracer experiments using [^{13}C]glucose and [^{13}C]glutamine were applied to *Mpc* knockdown cells, as this modeling approach has been shown to increase flux resolution throughout central carbon metabolism (Ahn and Antoniewicz, 2013). Although ATP-linked respiration and cell growth remained unchanged, we identified specific changes in amino acid and fatty acid metabolism that were recapitulated using the MPC inhibitor UK5099. Glucose metabolism in the TCA cycle was significantly decreased, but not completely, presumably due to incomplete knockdown, passive diffusion, or the presence of an alternate or nonfacilitated

transport mechanism. Rather than divert excess cytosolic pyruvate to lactate or alanine, this carbon was either secreted from cells as pyruvate or converted to serine. This latter activity may be driven by accumulation of glycolytic intermediates (Chaneton et al., 2012; Ye et al., 2012) or due to increased serine catabolism in mitochondria (Jain et al., 2012; Lewis et al., 2014). Notably, alanine levels were significantly decreased in *Mpc* knockdown cells, highlighting a role for mitochondrial pyruvate and mitochondrial alanine aminotransferase (ALT2) in mediating glutamine anaplerosis, which was previously described in cancer cells (Weinberg et al., 2010). The accumulation of aspartate in these cells provides evidence of the expected switch to rely on oxaloacetate and mitochondrial glutamic-oxaloacetic transaminase 2 (GOT2) to facilitate this process (Figure S1B). A similar response was observed in isolated retina treated with the MPC inhibitor Zaprinast (Du et al., 2013).

In addition to these metabolomic changes, we also observed increased amino acid and fatty acid oxidation upon inhibition of MPC. Elevated glutamine anaplerosis and oxidation are likely a consequence of decreased citrate synthase and oxidative IDH flux downstream of PDH while the ETC remained active (Fan et al., 2013; Le et al., 2012). We also observed a significant increase in BCAA oxidation upon MPC inhibition using hSKM cultures, which are of perhaps greater physiological relevance than C2C12 cells. Consistent with this change, Bricker et al. (2012) and Herzig et al. (2012) both observed growth defects in medium lacking leucine or valine in their characterizations of yeast with *Mpc* deletions. Mpc inhibition may potentiate oxidation of BCAAs or other amino acids that accumulate in the context of insulin resistance (Adams, 2011; Newgard et al., 2009; Wang et al., 2011). Citrate mass isotopomer labeling and flux estimations also highlighted a significant increase in flux through malic enzyme upon *Mpc* knockdown, which could provide additional reducing equivalents (NAD[P]H) within the matrix. These results are consistent with the severe growth defect previously observed in yeast with deletions in both *mpc1* and mitochondrial malic enzyme growing on glucose (Bricker et al., 2012), highlighting the remarkably conserved nature of metabolism across species.

An initial lack of fit observed in our *Mpc* knockdown model led us to hypothesize that fatty acid oxidation was increased under these conditions. This response was validated by tracing with [^{13}C]palmitate-BSA in myoblasts and cancer cells and using either shRNAs or UK5099 to inhibit mitochondrial pyruvate transport. Here, β-oxidation was presumably stimulated, in part, due to decreases in citrate and the downstream lipogenic intermediate malonyl-CoA, which inhibits CPT1 (McGarry et al., 1983). In this manner, pharmacological inhibition of the MPC could stimulate catabolic metabolism in muscle or liver.

Our analyses also more explicitly delineate the roles of MPC1 and MPC2 as components of the mitochondrial pyruvate transporter. Although strong evidence supports this functionality (Bricker et al., 2012; Divakaruni et al., 2013; Herzig et al., 2012), MPC-mediated regulation of pyruvate dehydrogenase (PDH) complex activity has been suggested as an alternative function of the MPC proteins (Halestrap, 2012). While our MFA results indicated that overall flux through PDH was decreased in Mpc2 knockdown cells, supplementation of pyruvate at concentrations expected to enter mitochondria through passive diffusion abrogated the increase in glutamine to fatty acid conversion. Furthermore, conversion of [^{13}C]pyruvate carbons to lipogenic AcCoA confirmed that this pyruvate was metabolized by PDH, since carbon atoms in oxaloacetate do not enter the AcCoA pool without PDH activity.

These results also demonstrate that MPC inhibition elicits a distinct metabolic phenotype compared to hypoxia or ETC inhibition. Whereas elevated glycolytic rates and reductive carboxylation are predominant modes of metabolism under such conditions (Metallo et al., 2012; Mullen et al., 2012; Scott et al., 2011; Wise et al., 2011), Mpc inhibition instead promoted oxidative glutaminolysis to fuel the mitochondrial AcCoA pool. Surprisingly, we observed no increase in reductive carboxylation flux. Fatty acid synthesis rates were also maintained upon *Mpc* knockdown, in contrast to that observed when comparing normoxic and hypoxic cell growth (Kamphorst et al., 2013; Metallo et al., 2012).

It is well established that oxidation of glucose and fatty acids are dynamically balanced in response to nutrient availability and hormonal control (Keung et al., 2013; Muoio et al., 2012), and disruptions of these processes are evident in metabolic and heart disease. Extensive studies support that inhibition of fatty acid oxidation, via genetic manipulation or pharmacologic intervention, can increase the rate of pyruvate oxidation (Fillmore and Lopaschuk, 2013). However, the converse principle has yet to be shown: that a reduction in pyruvate oxidation can stimulate β-oxidation. This may be partly due to the lack of a druggable therapeutic target. Our model, though, suggests that inhibition of mitochondrial pyruvate uptake can rewire cellular metabolism to boost fatty acid oxidation, which may provide an approach to further studies of the interplay between carbohydrate and fat metabolism. Given the importance of this metabolic control point, significant interest in identifying drugs that control MPC activity has emerged (Colca et al., 2013; Divakaruni et al., 2013; Du et al., 2013). The metabolic phenotype of MPC inhibition defined here using both shRNAs and UK5099 in cultured cell lines and hSKMs will provide a roadmap for molecular level validation of new compounds, facilitating the ability of researchers to identify drugs that target MPC versus other mitochondrial enzymes. Indeed, the phosphodiesterase inhibitor Zaprinast was recently demonstrated to inhibit mitochondrial pyruvate uptake. While Du et al. (2013) similarly observed an increase in aspartate levels, no evidence of glutaminolysis through malic enzyme was observed, potentially due to off-target effects on mitochondrial glutaminase (Elhammali et al., 2014). These findings highlight the need for systems-level analyses of metabolism to functionally validate gene function and drug specificity. In turn, the identification of selective compounds that influence mitochondrial substrate transport and utilization may provide therapeutic avenues to exploit the exquisite flexibility of these organelles.

EXPERIMENTAL PROCEDURES

Cell Culture and ^{13}C Tracing

C2C12, A549, and Huh7 cells were cultured in Dulbecco's modified Eagle's medium (DMEM) with 10% fetal bovine serum (FBS). Terminal differentiation

of C2C12 cells was initiated by 4-day culture in DMEM with 2% horse serum. Human skeletal muscle satellite cells were proliferated in SkFM (Lonza) and then differentiated to myotubes in MEMα supplemented with 2% FBS as described previously (Henry et al., 1995). For tracer and MFA studies, custom, phenol red-free DMEM or amino acid-free DMEM/F12 (for hSKMs) was formulated by replacing the substrate of interest with ^{13}C-labeled glucose, glutamine, pyruvate, or BCAAs (all from Cambridge Isotopes) with other components unlabeled. Cultures were washed with PBS before adding tracer media for 15–30 hr unless otherwise specified. Fatty acid oxidation studies were conducted using [U-$^{13}C_{16}$]palmitate noncovalently bound to fatty acid-free BSA. [U-$^{13}C_{16}$]palmitate-BSA was added to culture medium at 5% of the final volume (50 μM final concentration) with 1 mM carnitine in medium formulated with FBS that was delipidated using fumed silica (Sigma) according to the manufacturer's instructions.

Metabolic Flux Analysis

MFA was performed using the elementary metabolite unit-based software package INCA. Inputs to the model include the chemical reactions and atom transitions of central carbon metabolism, measured substrate extracellular fluxes, the identity of the ^{13}C-labeled tracers, and mass isotopomer distributions of select intracellular metabolites. Assumptions are listed in the Supplemental Experimental Procedures.

Oxygen Consumption Measurements

Respiration was measured in adherent monolayers of C2C12 myocytes using a Seahorse XF96 Analyzer. Myoblasts were plated at 1 × 10^4 cells/well and grown for 2 days. Cells were assayed in unbuffered DMEM (Sigma #D5030) supplemented with 8 mM glucose and 3 mM glutamine. Unless stated in the figure legend, pyruvate was omitted from the assay medium. ATP-linked respiration was calculated as the oxygen consumption rate sensitive to 2 μg/ml oligomycin. Maximal respiration was calculated as the difference between protonophore-stimulated respiration (measured as the highest rate from sequential additions of FCCP; final concentrations between 400 and 800 nM) and nonmitochondrial respiration (measured after addition of 2 μM rotenone and 2 μM antimycin A). Where indicated, etomoxir (20 μM) or BPTES (3 μM) was added to the plate 20 min prior to basal respiration measurements. Respiration in permeabilized cells (1 nM XF PMP, Seahorse Bioscience) was measured in cells offered 5 mM pyruvate, 0.5 mM malate, 2 mM DCA, 2 μg/ml oligomycin, and 400 nM FCCP. All data are mean ± SEM of at least four biological replicates (with a minimum of five technical replicates per experiment). Statistical analysis was conducted using ANOVA of repeated measures with Dunnett's post hoc test. Where appropriate, the square root of normalized data was analyzed.

Metabolite Extraction and GC/MS Analysis

At the conclusion of a tracer experiment, the tracer media was removed from the culture wells, the cells were washed with a saline solution, and the bottom of the well was covered with cold methanol to lyse the cells and halt metabolism. Water containing norvaline at 5 μg/ml was charged to each well at a volume ratio of 1:2.5 relative to the methanol. The bottom of each well was scraped with a 1,000 μl pipette tip, and the cells were collected in 1.5 ml tubes. Cold chloroform containing 2 μg/ml of heptadodecnaoate was added to each sample at a 1:1 volume ratio relative to the methanol. The mixtures were vortexed, and the polar and nonpolar layers were separated and evaporated after centrifugation. Details of the derivatization process can be found in the Supplemental Experimental Procedures.

Derivatized metabolites were analyzed using a DB-35MS column (30 m × 0.25 mm internal diameter × 0.25 μm; Agilent J&W Scientific) in an Agilent 7890A gas chromatograph coupled to a 5975C mass spectrometer. Details of the chromatography method and mass spectrometry scanning parameters can be found in the Supplemental Experimental Procedures.

Human Subjects

All human skeletal muscle biopsies were obtained with approval from the University of California San Diego's Committee on Human Investigation. All donors provided informed written consent after listening to an explanation of the protocol.

SUPPLEMENTAL INFORMATION

Supplemental Information includes Supplemental Experimental Procedures, four figures, and three tables and can be found with this article online at http://dx.doi.org/10.1016/j.molcel.2014.09.024.

ACKNOWLEDGMENTS

We thank Sandra E. Wiley, Hui Zhang, Ryan LaCroix, Spencer Lee, and Mehmet G. Badur for technical assistance and members of the Metallo lab for discussions. This work was supported, in part, by NIH grants P30DK063491, R01CA188652, and T32HL105373 (to N.M.V.), DOD grant W81XWH-13-1-0105, a Hellman Faculty Fellowship, and a Searle Scholar Award (to C.M.M.), a grant from the Medical Research Service, Department of Veterans Affairs, VA San Diego Healthcare System (to R.R.H.), and NIH grant R01NS087611 and Seahorse Bioscience (to A.N.M.). A.N.M. and A.S.D. are consultants for Seahorse Bioscience.

Received: May 8, 2014
Revised: August 26, 2014
Accepted: September 25, 2014
Published: October 30, 2014

REFERENCES

Adams, S.H. (2011). Emerging perspectives on essential amino acid metabolism in obesity and the insulin-resistant state. Adv Nutr *2*, 445–456.

Ahn, W.S., and Antoniewicz, M.R. (2011). Metabolic flux analysis of CHO cells at growth and non-growth phases using isotopic tracers and mass spectrometry. Metab. Eng. *13*, 598–609.

Ahn, W.S., and Antoniewicz, M.R. (2013). Parallel labeling experiments with [1,2-(13)C]glucose and [U-(13)C]glutamine provide new insights into CHO cell metabolism. Metab. Eng. *15*, 34–47.

Antoniewicz, M.R., Kelleher, J.K., and Stephanopoulos, G. (2006). Determination of confidence intervals of metabolic fluxes estimated from stable isotope measurements. Metab. Eng. *8*, 324–337.

Bakker, E.P., and van Dam, K. (1974). The movement of monocarboxylic acids across phospholipid membranes: evidence for an exchange diffusion between pyruvate and other monocarboxylate ions. Biochim. Biophys. Acta *339*, 285–289.

Bricker, D.K., Taylor, E.B., Schell, J.C., Orsak, T., Boutron, A., Chen, Y.C., Cox, J.E., Cardon, C.M., Van Vranken, J.G., Dephoure, N., et al. (2012). A mitochondrial pyruvate carrier required for pyruvate uptake in yeast, Drosophila, and humans. Science *337*, 96–100.

Chaneton, B., Hillmann, P., Zheng, L., Martin, A.C., Maddocks, O.D., Chokkathukalam, A., Coyle, J.E., Jankevics, A., Holding, F.P., Vousden, K.H., et al. (2012). Serine is a natural ligand and allosteric activator of pyruvate kinase M2. Nature *491*, 458–462.

Clark, J.B., and Land, J.M. (1974). Differential effects of 2-oxo acids on pyruvate utilization and fatty acid synthesis in rat brain. Biochem. J. *140*, 25–29.

Colca, J.R., McDonald, W.G., Cavey, G.S., Cole, S.L., Holewa, D.D., Brightwell-Conrad, A.S., Wolfe, C.L., Wheeler, J.S., Coulter, K.R., Kilkuskie, P.M., et al. (2013). Identification of a mitochondrial target of thiazolidinedione insulin sensitizers (mTOT)—relationship to newly identified mitochondrial pyruvate carrier proteins. PLoS ONE *8*, e61551.

Cunnane, S., Nugent, S., Roy, M., Courchesne-Loyer, A., Croteau, E., Tremblay, S., Castellano, A., Pifferi, F., Bocti, C., Paquet, N., et al. (2011). Brain fuel metabolism, aging, and Alzheimer's disease. Nutrition *27*, 3–20.

Currie, E., Schulze, A., Zechner, R., Walther, T.C., and Farese, R.V., Jr. (2013). Cellular fatty acid metabolism and cancer. Cell Metab. *18*, 153–161.

DeFronzo, R.A., and Tripathy, D. (2009). Skeletal muscle insulin resistance is the primary defect in type 2 diabetes. Diabetes Care *32* (*Suppl 2*), S157–S163.

Divakaruni, A.S., Wiley, S.E., Rogers, G.W., Andreyev, A.Y., Petrosyan, S., Loviscach, M., Wall, E.A., Yadava, N., Heuck, A.P., Ferrick, D.A., et al. (2013). Thiazolidinediones are acute, specific inhibitors of the mitochondrial pyruvate carrier. Proc. Natl. Acad. Sci. USA *110*, 5422–5427.

Du, J., Cleghorn, W.M., Contreras, L., Lindsay, K., Rountree, A.M., Chertov, A.O., Turner, S.J., Sahaboglu, A., Linton, J., Sadilek, M., et al. (2013). Inhibition of mitochondrial pyruvate transport by zaprinast causes massive accumulation of aspartate at the expense of glutamate in the retina. J. Biol. Chem. *288*, 36129–36140.

Elhammali, A., Ippolito, J.E., Collins, L., Crowley, J., Marasa, J., and Piwnica-Worms, D. (2014). A high-throughput fluorimetric assay for 2-hydroxyglutarate identifies Zaprinast as a glutaminase inhibitor. Cancer Discov *4*, 828–839.

Fan, J., Kamphorst, J.J., Mathew, R., Chung, M.K., White, E., Shlomi, T., and Rabinowitz, J.D. (2013). Glutamine-driven oxidative phosphorylation is a major ATP source in transformed mammalian cells in both normoxia and hypoxia. Mol. Syst. Biol. *9*, 712.

Fillmore, N., and Lopaschuk, G.D. (2013). Targeting mitochondrial oxidative metabolism as an approach to treat heart failure. Biochim. Biophys. Acta *1833*, 857–865.

Halestrap, A.P. (1975). The mitochondrial pyruvate carrier. Kinetics and specificity for substrates and inhibitors. Biochem. J. *148*, 85–96.

Halestrap, A.P. (2012). The mitochondrial pyruvate carrier: has it been unearthed at last? Cell Metab. *16*, 141–143.

Halestrap, A.P., and Denton, R.M. (1974). Specific inhibition of pyruvate transport in rat liver mitochondria and human erythrocytes by alpha-cyano-4-hydroxycinnamate. Biochem. J. *138*, 313–316.

Henry, R.R., Abrams, L., Nikoulina, S., and Ciaraldi, T.P. (1995). Insulin action and glucose metabolism in nondiabetic control and NIDDM subjects. Comparison using human skeletal muscle cell cultures. Diabetes *44*, 936–946.

Herzig, S., Raemy, E., Montessuit, S., Veuthey, J.L., Zamboni, N., Westermann, B., Kunji, E.R., and Martinou, J.C. (2012). Identification and functional expression of the mitochondrial pyruvate carrier. Science *337*, 93–96.

Hildyard, J.C., Ammälä, C., Dukes, I.D., Thomson, S.A., and Halestrap, A.P. (2005). Identification and characterisation of a new class of highly specific and potent inhibitors of the mitochondrial pyruvate carrier. Biochim. Biophys. Acta *1707*, 221–230.

Jain, M., Nilsson, R., Sharma, S., Madhusudhan, N., Kitami, T., Souza, A.L., Kafri, R., Kirschner, M.W., Clish, C.B., and Mootha, V.K. (2012). Metabolite profiling identifies a key role for glycine in rapid cancer cell proliferation. Science *336*, 1040–1044.

Kamphorst, J.J., Cross, J.R., Fan, J., de Stanchina, E., Mathew, R., White, E.P., Thompson, C.B., and Rabinowitz, J.D. (2013). Hypoxic and Ras-transformed cells support growth by scavenging unsaturated fatty acids from lysophospholipids. Proc. Natl. Acad. Sci. USA *110*, 8882–8887.

Kerr, D.S. (2013). Review of clinical trials for mitochondrial disorders: 1997-2012. Neurotherapeutics *10*, 307–319.

Keung, W., Ussher, J.R., Jaswal, J.S., Raubenheimer, M., Lam, V.H., Wagg, C.S., and Lopaschuk, G.D. (2013). Inhibition of carnitine palmitoyltransferase-1 activity alleviates insulin resistance in diet-induced obese mice. Diabetes *62*, 711–720.

Kharroubi, A.T., Masterson, T.M., Aldaghlas, T.A., Kennedy, K.A., and Kelleher, J.K. (1992). Isotopomer spectral analysis of triglyceride fatty acid synthesis in 3T3-L1 cells. Am. J. Physiol. *263*, E667–E675.

Kim, J.W., Tchernyshyov, I., Semenza, G.L., and Dang, C.V. (2006). HIF-1-mediated expression of pyruvate dehydrogenase kinase: a metabolic switch required for cellular adaptation to hypoxia. Cell Metab. *3*, 177–185.

Le, A., Lane, A.N., Hamaker, M., Bose, S., Gouw, A., Barbi, J., Tsukamoto, T., Rojas, C.J., Slusher, B.S., Zhang, H., et al. (2012). Glucose-independent glutamine metabolism via TCA cycling for proliferation and survival in B cells. Cell Metab. *15*, 110–121.

Lewis, C.A., Parker, S.J., Fiske, B.P., McCloskey, D., Gui, D.Y., Green, C.R., Vokes, N.I., Feist, A.M., Vander Heiden, M.G., and Metallo, C.M. (2014). Tracing compartmentalized NADPH metabolism in the cytosol and mitochondria of mammalian cells. Mol. Cell *55*, 253–263.

McGarry, J.D., Mills, S.E., Long, C.S., and Foster, D.W. (1983). Observations on the affinity for carnitine, and malonyl-CoA sensitivity, of carnitine palmitoyltransferase I in animal and human tissues. Demonstration of the presence of malonyl-CoA in non-hepatic tissues of the rat. Biochem. J. *214*, 21–28.

Metallo, C.M., and Vander Heiden, M.G. (2013). Understanding metabolic regulation and its influence on cell physiology. Mol. Cell *49*, 388–398.

Metallo, C.M., Gameiro, P.A., Bell, E.L., Mattaini, K.R., Yang, J., Hiller, K., Jewell, C.M., Johnson, Z.R., Irvine, D.J., Guarente, L., et al. (2012). Reductive glutamine metabolism by IDH1 mediates lipogenesis under hypoxia. Nature *481*, 380–384.

Mullen, A.R., Wheaton, W.W., Jin, E.S., Chen, P.H., Sullivan, L.B., Cheng, T., Yang, Y., Linehan, W.M., Chandel, N.S., and DeBerardinis, R.J. (2012). Reductive carboxylation supports growth in tumour cells with defective mitochondria. Nature *481*, 385–388.

Muoio, D.M., Noland, R.C., Kovalik, J.P., Seiler, S.E., Davies, M.N., DeBalsi, K.L., Ilkayeva, O.R., Stevens, R.D., Kheterpal, I., Zhang, J., et al. (2012). Muscle-specific deletion of carnitine acetyltransferase compromises glucose tolerance and metabolic flexibility. Cell Metab. *15*, 764–777.

Murphy, T.A., Dang, C.V., and Young, J.D. (2013). Isotopically nonstationary 13C flux analysis of Myc-induced metabolic reprogramming in B-cells. Metab. Eng. *15*, 206–217.

Newgard, C.B., An, J., Bain, J.R., Muehlbauer, M.J., Stevens, R.D., Lien, L.F., Haqq, A.M., Shah, S.H., Arlotto, M., Slentz, C.A., et al. (2009). A branched-chain amino acid-related metabolic signature that differentiates obese and lean humans and contributes to insulin resistance. Cell Metab. *9*, 311–326.

Papa, S., and Paradies, G. (1974). On the mechanism of translocation of pyruvate and other monocarboxylic acids in rat-liver mitochondria. Eur. J. Biochem. *49*, 265–274.

Papa, S., Francavilla, A., Paradies, G., and Meduri, B. (1971). The transport of pyruvate in rat liver mitochondria. FEBS Lett. *12*, 285–288.

Papandreou, I., Cairns, R.A., Fontana, L., Lim, A.L., and Denko, N.C. (2006). HIF-1 mediates adaptation to hypoxia by actively downregulating mitochondrial oxygen consumption. Cell Metab. *3*, 187–197.

Patterson, J.N., Cousteils, K., Lou, J.W., Manning Fox, J.E., MacDonald, P.E., and Joseph, J.W. (2014). Mitochondrial metabolism of pyruvate is essential for regulating glucose-stimulated insulin secretion. J. Biol. Chem. *289*, 13335–13346.

Rosenthal, J., Angel, A., and Farkas, J. (1974). Metabolic fate of leucine: a significant sterol precursor in adipose tissue and muscle. Am. J. Physiol. *226*, 411–418.

Scott, D.A., Richardson, A.D., Filipp, F.V., Knutzen, C.A., Chiang, G.G., Ronai, Z.A., Osterman, A.L., and Smith, J.W. (2011). Comparative metabolic flux profiling of melanoma cell lines: beyond the Warburg effect. J. Biol. Chem. *286*, 42626–42634.

Sugden, M.C., Zariwala, M.G., and Holness, M.J. (2009). PPARs and the orchestration of metabolic fuel selection. Pharmacol. Res. *60*, 141–150.

Tennant, D.A., Durán, R.V., and Gottlieb, E. (2010). Targeting metabolic transformation for cancer therapy. Nat. Rev. Cancer *10*, 267–277.

Vigueira, P.A., McCommis, K.S., Schweitzer, G.G., Remedi, M.S., Chambers, K.T., Fu, X., McDonald, W.G., Cole, S.L., Colca, J.R., Kletzien, R.F., et al. (2014). Mitochondrial pyruvate carrier 2 hypomorphism in mice leads to defects in glucose-stimulated insulin secretion. Cell Rep *7*, 2042–2053.

Wang, T.J., Larson, M.G., Vasan, R.S., Cheng, S., Rhee, E.P., McCabe, E., Lewis, G.D., Fox, C.S., Jacques, P.F., Fernandez, C., et al. (2011). Metabolite profiles and the risk of developing diabetes. Nat. Med. *17*, 448–453.

Weinberg, F., Hamanaka, R., Wheaton, W.W., Weinberg, S., Joseph, J., Lopez, M., Kalyanaraman, B., Mutlu, G.M., Budinger, G.R., and Chandel, N.S. (2010). Mitochondrial metabolism and ROS generation are essential for Kras-mediated tumorigenicity. Proc. Natl. Acad. Sci. USA *107*, 8788–8793.

Wise, D.R., Ward, P.S., Shay, J.E., Cross, J.R., Gruber, J.J., Sachdeva, U.M., Platt, J.M., DeMatteo, R.G., Simon, M.C., and Thompson, C.B. (2011). Hypoxia promotes isocitrate dehydrogenase-dependent carboxylation of α-ketoglutarate to citrate to support cell growth and viability. Proc. Natl. Acad. Sci. USA *108*, 19611–19616.

Yao, J., Rettberg, J.R., Klosinski, L.P., Cadenas, E., and Brinton, R.D. (2011). Shift in brain metabolism in late onset Alzheimer's disease: implications for biomarkers and therapeutic interventions. Mol. Aspects Med. *32*, 247–257.

Ye, J., Mancuso, A., Tong, X., Ward, P.S., Fan, J., Rabinowitz, J.D., and Thompson, C.B. (2012). Pyruvate kinase M2 promotes de novo serine synthesis to sustain mTORC1 activity and cell proliferation. Proc. Natl. Acad. Sci. USA *109*, 6904–6909.

Yoo, H., Antoniewicz, M.R., Stephanopoulos, G., and Kelleher, J.K. (2008). Quantifying reductive carboxylation flux of glutamine to lipid in a brown adipocyte cell line. J. Biol. Chem. *283*, 20621–20627.

Young, J.D. (2014). INCA: a computational platform for isotopically non-stationary metabolic flux analysis. Bioinformatics *30*, 1333–1335.

Zamboni, N., Fendt, S.M., Rühl, M., and Sauer, U. (2009). (13)C-based metabolic flux analysis. Nat. Protoc. *4*, 878–892.